2018

Measurement Of Pressure Profile Of Vortex Flashing Flows In Convergent-Divergent Nozzles

Jingwei Zhu
ACRC, University of Illinois at Urbana-Champaign, jzhu50@illinois.edu

Stefan Elbel
elbel@illinois.edu

Measurement Of Pressure Profile Of Vortex Flashing Flows In Convergent-Divergent Nozzles

Jingwei ZHU, Stefan ELBEL*

Department of Mechanical Science and Engineering,
University of Illinois at Urbana-Champaign,
1206 West Green Street, Urbana, IL, 61801, USA
Phone: (217) 244-1531, Fax: (217) 333-1942, Email: elbel@illinois.edu

* Corresponding Author

ABSTRACT

Vortex control is a novel two-phase convergent-divergent nozzle restrictiveness control mechanism which requires no change to the physical dimensions of the nozzle geometry. The control is achieved by adjustable nozzle inlet vortex. This novel control mechanism can potentially provide flow control with less sacrifice of nozzle efficiency, which is extremely important for ejector cooling cycle performance. It is also less vulnerable to clogging since the flow control is achieved without changing the flow area. However, the underlying mechanism behind the vortex control is still unclear. Measurement of the pressure profile of the vortex flashing flows in convergent-divergent nozzles under different conditions can provide more insights into the vortex nozzle flows and help to explain the vortex control mechanism. It also provides validation for modeling of vortex flashing flows. In this study, the experimental investigation of the pressure profile of the vortex flashing flows is presented. For initially subcooled conditions the pressure drop in the divergent part of the nozzle has been increased due to the vortex. This is mainly due to the more vapor generation in the divergent part caused by the applied vortex. Since the fluid is single-phase liquid in the convergent part of the nozzle, with elevated pressure at the throat and constant inlet conditions, the nozzle mass flow rate is therefore reduced. Vapor quality at different axial locations relative to the nozzle throat has been estimated with a proposed 1D model for initially subcooled conditions based on the measured pressure profile and mass flow rates. It has been shown that the applied vortex makes the outflow much closer to thermodynamic equilibrium than without vortex. By the introduction of inlet vortex, the isentropic efficiency of the nozzle has been improved from 29% to 55%.

1. INTRODUCTION

Refrigerant flow control with expansion devices can provide significant improvement to the performance of air conditioning and refrigeration systems under changing working conditions. The most widely used expansion devices that regulate the refrigerant flow into the evaporators are thermostatic expansion valves (TXV) and electronic expansion valves (EEV). In systems with subcritical heat rejection, they control the superheating level at the evaporator outlet which leads to the best use of evaporator under each condition and prevents unevaporated refrigerant liquid from reaching the compressor. The flow control is accomplished by varying the expansion valve opening.

Zhu and Elbel (2016, 2017, 2018a) were the first to experimentally investigate the influence of nozzle inlet vortex on the nozzle restrictiveness on initially subcooled flashing flow expanded through convergent-divergent nozzles. This novel two-phase nozzle restrictiveness control mechanism by adjustable nozzle inlet vortex, called vortex control, requires no change to the physical dimensions of the nozzle geometry. A nozzle with inlet vortex was called vortex nozzle (or swirl nozzle). Zhu and Elbel's experiments on vortex nozzle with initially subcooled R134a showed that the strength of the nozzle inlet vortex can change the restrictiveness of the two-phase convergent-

divergent nozzle without the need of changing the nozzle geometry. The nozzle becomes more restrictive as the strength of the vortex increases. With vortex control, the mass flow rate can be reduced by 42% under the same inlet and outlet conditions (Zhu and Elbel, 2018a). The control range of inlet pressures and mass flow rates that can be achieved by vortex control appears to be large enough to be suitable for numerous technical applications. This novel mechanism can potentially provide flow control with less sacrifice of nozzle efficiency, which is extremely important for ejector cooling cycle performance. It is also less vulnerable to clogging since the flow control is achieved without changing the flow area. A variety of different expansion devices, in addition to ejectors, could potentially benefit from this new control mechanism, including actively controlled flow metering devices for superheat control in subcritical applications or high-side pressure control in transcritical systems. Furthermore, the new vortex control mechanism can possibly lead to alternative self−regulating expansion valve designs.

Through the literature review, it was found that flashing flow of initially subcooled or saturated fluid was studied without vortex applied, and vortex flow was mostly studied without phase change or the focus of research was on the spray dynamics and atomization characteristics. Little knowledge is available regarding the underlying mechanism behind the control effect of vortex on the flashing flow rate. In this study, measurement of the pressure profile of the vortex flashing flows in convergent-divergent nozzles under different conditions was conducted, which can provide more insights into the vortex nozzle flows and help to explain the vortex control effect. It also provides validation for modeling of vortex flashing flows. In the following sections, the test facility for measurement of the pressure profile of the vortex flashing flow will be introduced first. The nozzle pressure profile under different inlet (subcooled liquid/two-phase, with/without inlet vortex) and outlet conditions will be presented and discussed. The vortex control effect will be explained with the insight provided by the pressure profile measurements.

2. TEST FACILITY

Nozzle with controllable vortex at the nozzle inlet have been designed and manufactured for experiments, as shown in Figure 1. The vortex nozzle is composed of three components: a T-shaped part made of brass, a sleeve and a nozzle, both made of an optically clear resin and manufactured with a Stereo Lithography Apparatus (SLA). The tee-shaped part serves as the vortex generator. The tangential inlet on the tee allows flow to be injected tangentially and mix with the axial flow, thus creating a vortex. The tee and the nozzle are joined by a conical thread and sealed by epoxy adhesive. The other conical thread on the nozzle is for connection with a visualization chamber. The sleeve is designed to provide a smooth transition between the tee part and the nozzle. The gap between the sleeve and the nozzle is minimized and therefore the additional disturbance introduced to the flow. The inner diameter of the sleeve is the same as that of the nozzle entrance. There is a tangential inlet on the sleeve. The tangential inlet on the tee and the tangential inlet on the sleeve are coaxial and have the same inner diameter. For visualization purpose, the flow needs to travel a long distance from the tangential inlet to the starting point of the convergent part of the nozzle. This distance is called vortex decay distance, as shown in Figure 1 with the letter ‘g’. Because of the fluid viscosity and turbulence, vortex strength will decay over this distance.

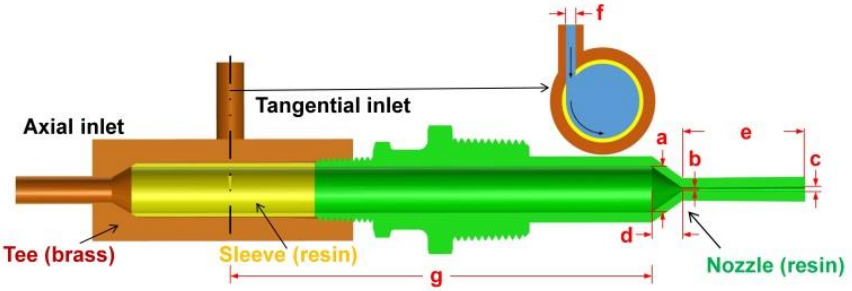

Figure 1: Vortex nozzle composed of tee, sleeve and convergent-divergent nozzle

The cross-sectional view of the nozzle with pressure measurement channels is presented in Figure 2. There are six pressure measurement channels in total and the axial locations of the channel tips are presented with numbers 2~7 in Figure 2. The tips of these channels in contact with the nozzle flow are of square shape with edge length of approximately 0.25 mm. This is the minimum channel tip size that can be 3D-printed without any clogging. Numbers 1 and 8 represent the nozzle inlet and outlet pressures, respectively. The axial locations of these measurement channel tips relative to the nozzle throat are presented in Table 1. Only two of the channels are shown in the cross-sectional view in Figure 2.

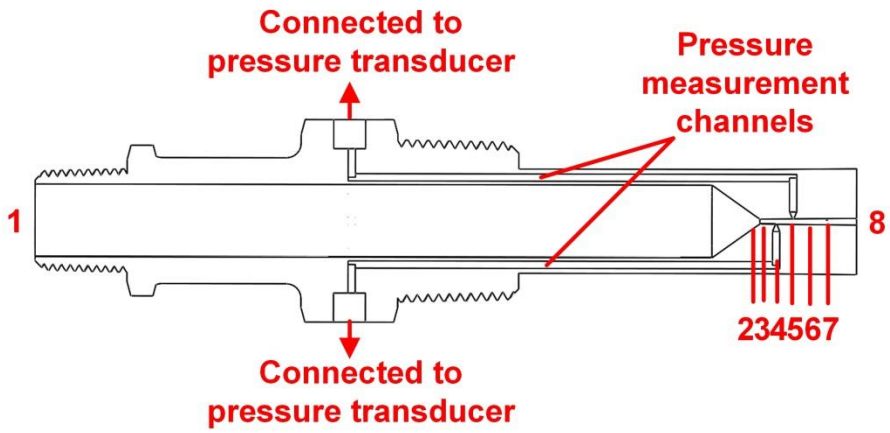

Figure 2: Cross-sectional view of the convergent-divergent nozzle with pressure measurement channels

Table 1: Axial locations of the measurement channel tips relative to the nozzle throat

Pressure measurement channel number	2	3	4	5	6	7
Axial location of the tip relative to the nozzle throat (mm)	-1.00	0.57	3.37	6.87	10.37	13.88

Important dimensions of the tested vortex nozzle have been summarized in Table 2 and these dimensions are shown with corresponding letters in Figure 1.

Table 2: Geometric parameters of tested vortex nozzle (shown with corresponding letters in Figure 1)

(a) Nozzle inlet diameter (mm)	15.0
(b) Nozzle throat diameter (mm)	1.02
(c) Nozzle outlet diameter (mm)	1.37
(d) Nozzle convergent part length (mm)	9.9
(e) Nozzle divergent part length (mm)	20.0
(f) Tangential inlet inner diameter (mm)	2.0
(g) Vortex decay distance (mm)	168.0

The layout of the experimental facility for measurement of pressure profile of vortex flashing flows in convergent-divergent nozzles is shown in Figure 3. A pumped-refrigerant-loop was used for adjustment of nozzle test conditions. The working fluid was refrigerant R134a. A visualization chamber was built from clear PVC pipe. The temperature readings were all obtained from ungrounded Type-T immersion thermocouples. The measured temperatures are regarded as total temperatures. Absolute pressures were read by piezo-electric pressure transducers. Pressures and temperatures in the upstream of the nozzle axial and tangential inlet control valves were measured. Pressures in the downstream of the control valves were also measured. For tests with two-phase flow at the nozzle inlet, the fluid in the upstream of the inlet control valves was single-phase liquid, while in the downstream of the control valves the fluid became two-phase after the expansion. The nozzle inlet vapor quality was calculated by the measured pressure and temperature of the single-phase liquid in the upstream of the valves and the pressure in the downstream of the valves and assuming isenthalpic expansion. The axial inlet pressure was slightly lower than the tangential inlet pressure. This pressure difference was caused as a result of the refrigerant flowing through the tangential inlet with relatively small inner diameter (2.0 mm). The differences between the vortex nozzle axial inlet pressures and tangential inlet pressures were within 10 kPa when the tangential inlet mass flow rate is less than 13.0 g s^{-1} (single-phase liquid). The pressure difference increases to 28 kPa when the tangential inlet mass flow rate is 20.5 g s^{-1} (single-phase liquid). The axial inlet pressure is assumed to be the nozzle inlet pressure P_{in}. The pressure at different axial locations of the nozzle and the nozzle outlet P_{out} was measured as well. The temperature difference between the axial and tangential inlets was kept within 0.5 °C when both tangential and axial inlets are open. In order to achieve this small temperature difference, test results for too small axial or tangential inlet mass flow rate are not available since heat losses in the tubing significantly increase the temperature difference between the two inlets when one of the flow rates is too small even with insulation. The axial inlet temperature is assumed to be the nozzle inlet temperature T_{in} when both inlets are open. When one of the inlets is fully closed, the open inlet temperature is assumed to be T_{in}. The total mass flow rate $\dot{m}_{total}$ and the nozzle axial inlet mass flow rate $\dot{m}_{axial}$ were measured

by Coriolis-type mass flow meters. The nozzle's tangential inlet mass flow rate $\dot{m}_{tangential}$ can be calculated by subtracting the nozzle axial inlet mass flow rate from the total mass flow rate. The ratio of the nozzle tangential inlet mass flow rate to the total mass flow rate was adjusted by two valves. The larger the ratio is, the large the vortex strength is for the same total mass flow rate. In this paper, the vortex strength is defined as the ratio of the nozzle tangential inlet mass flow rate to the total mass flow rate, which can be expressed as shown in Equation 1:

$$VS = \dot{m}_{tangential}/\dot{m}_{total} \quad (1)$$

Different nozzle inlet pressures were achieved by adjusting the heating water temperature, pump speed, and inlet control valves. The nozzle outlet pressure can be adjusted by a valve installed downstream of the nozzle. For all tests with subcooled liquid at the nozzle inlet, the sight glass installed at the nozzle inlet and the transparent body of the nozzle allows for visual confirmation that no bubbles are present at the nozzle inlet, which provides ultimate confirmation for inlet subcooling.

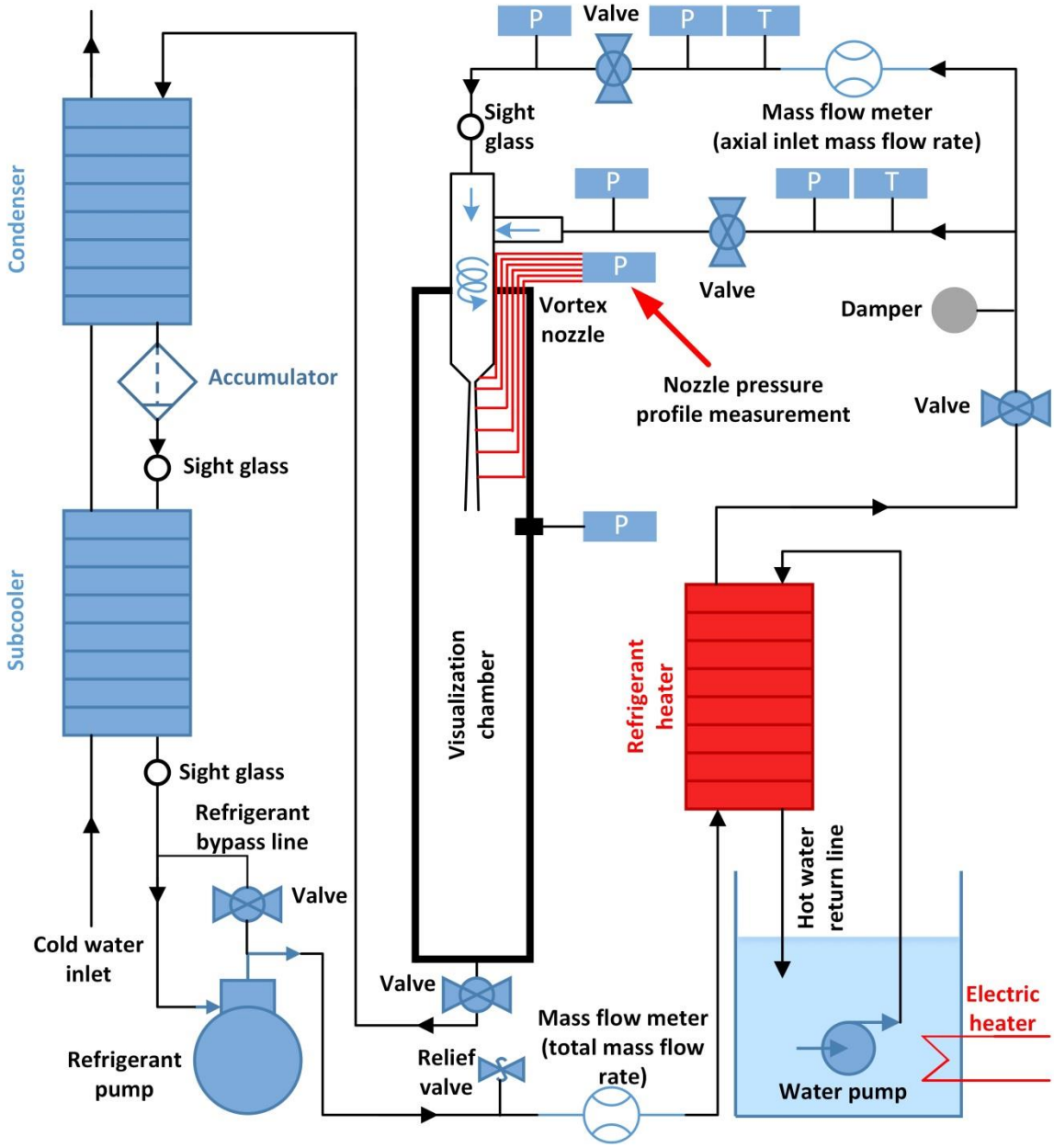

Figure 3: Experimental facility for measurement of pressure profile of vortex flashing flows in convergent-divergent nozzles

3. RESULTS AND DISCUSSION

The nozzle was first tested under the conditions P_{in}= 925 kPa, T_{in}=36.0 °C, P_{out}=615 kPa without/with maximum inlet vortex (VS=1) and the conditions P_{in}= 1018 kPa, T_{in}=36.0 °C, P_{out}=615 kPa with maximum inlet vortex. The pressure profile and average axial pressure gradient (dP/dx) at different axial locations of the nozzle are presented in Figure 4.

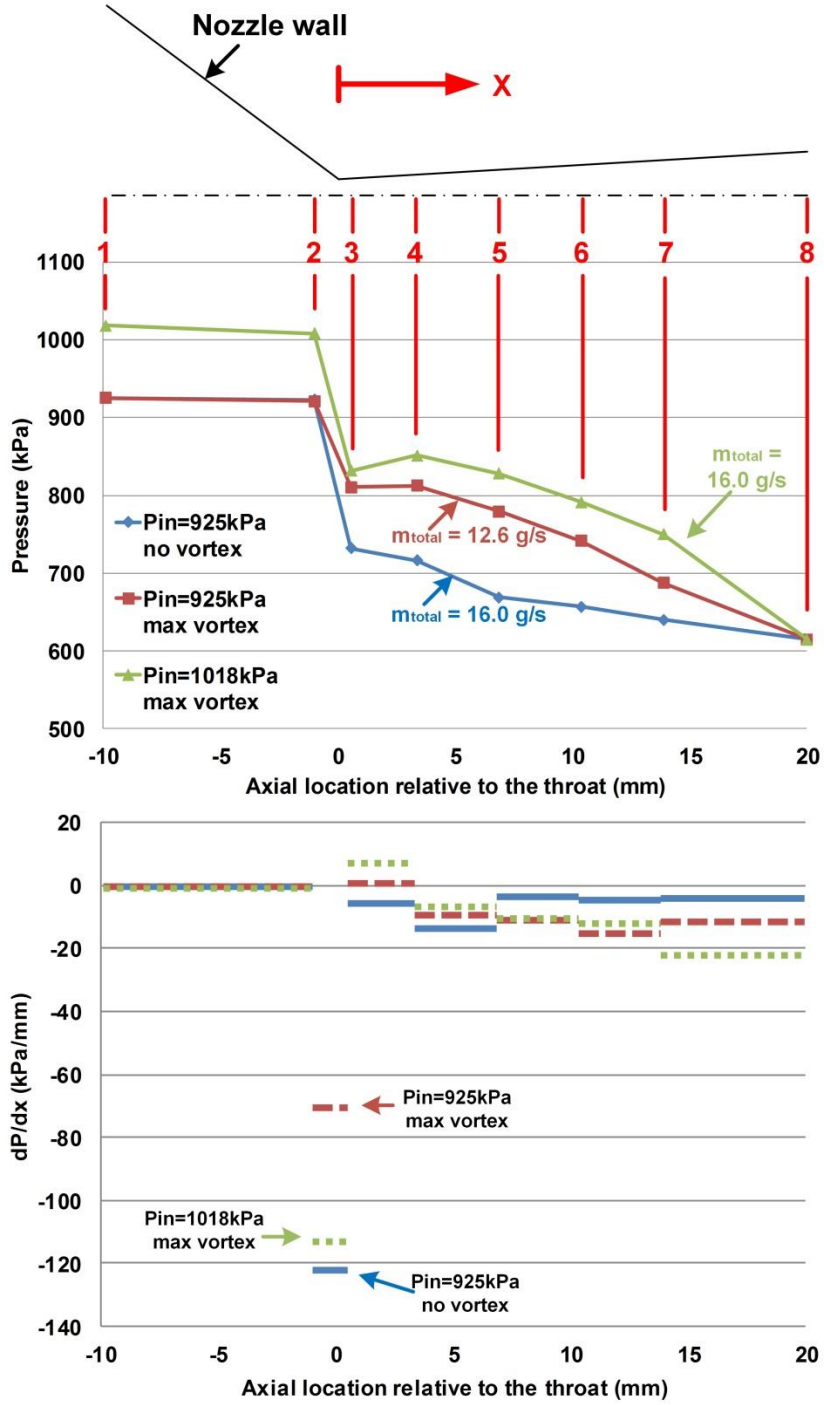

Figure 4: Pressure and average axial pressure gradient at different axial locations of the nozzle when T_{in}=36.0 °C and P_{out}=615 kPa

With P_{in}=925 kPa (approximately 0.5 °C inlet subcooling) and no inlet vortex, pressure in the divergent part of the nozzle keeps decreasing towards the downstream which suggests that the flow is accelerating. If there is single-phase liquid only in the divergent part, liquid will decelerate due to the increase of cross-sectional area and pressure may rise. The flow acceleration and pressure drop in the divergent part are mainly due to the vapor generation.

With inlet vortex strength of 1 and with the same inlet and outlet pressure and temperature conditions as the above case, nozzle mass flow rate has been reduced significantly from 16.0 g/s to 12.6 g/s. Meanwhile, the pressure drop in the divergent part has been increased due to the vortex. The pressure difference between locations 3 and 8 is 116.9 kPa when there is no inlet vortex and is increased to 195.6 kPa when there is maximum vortex applied. It is believed that this is mainly due to more vapor generation in the divergent part caused by the applied vortex. Due to the much lower density of vapor compared to the liquid, when vortex is applied vapor bubbles are driven towards the nozzle center. Sensible heat of the liquid closer to the nozzle center can now be more utilized for bubble growth. Due to the more available liquid sensible heat, after the introduction of inlet vortex, vapor generation in the nozzle divergent part has thus been increased (Zhu and Elbel, 2018b). It has been observed in previous flow visualization that in the convergent part of the nozzle, the fluid is single-phase liquid. With elevated pressure at the throat and constant inlet conditions, the nozzle mass flow rate is therefore reduced.

Larger magnitude of pressure dropping gradient has been observed betweem locations 5&6, 6&7, and 7&8 with maximum inlet vortex compared to that of the case with no inlet vortex, even when the nozzle mass flow rate with inlet vortex is much smaller. These three segments are the major contributor to the larger pressure difference in the divergent part when maximum vortex is applied. On the contrary, the pressure gradient between locations 3&4 is slightly higher than zero when there is maximum vortex and is negative when there is no vortex. This is because as pressure has been elevated near the throat due to the larger pressure drop in the downstream when vortex is applied, liquid superheat becomes smaller and less vapor can be generated between locations 3&4. As a result, the fluid behaves more like single-phase liquid and pressure rise in the divergent part near the throat is observed.

In order to have a fairer comparison of pressure and average axial pressure gradient profiles in the nozzle, another inlet condition has been considered (P_{in}=1018 kPa, T_{in}=36.0 °C) when maximum vortex is applied such that the total nozzle mass flow rate is equal to that of the case with no vortex and P_{in} =925 kPa (both are 16.0 g/s). For the same mass flow rate, pressure dropping gradient between locations 7&8 when there is maximum vortex is 22.0 kPa/mm which is much larger than 4.1 kPa/mm for the case with no vortex. The applied vortex increases the vapor generation in the divergent part of the nozzle, especially in the downstream part, and therefore much larger pressure dropping gradient is seen between locations 7&8. Due to the elevated pressure near the throat when maximum vortex is applied, vapor generation is suppressed between locations 3&4, and thus significant pressure rise (19.6 kPa) has been observed. This pressure rise seems to be the bottleneck of achieving larger vortex control range. If the pressure does not rise or even drops between locations 3&4 while the downstream pressure remain unchanged, it can be expected that the nozzle mass flow rate can potentially be further reduced and larger vortex control range can be achieved. For the same mass flow rate, when there is no vortex, pressure drops by 15.5 kPa.

Figure 5 shows the influence of inlet vortex strength on the pressure at different axial locations of the nozzle with P_{in}=1035 kPa, T_{in}=40.0 °C, and P_{out}=680 kPa. It can be observed that as inlet vortex strength starts to increase from 0 to 0.34, the pressure dropping gradient near the nozzle outlet (between locations 7&8) starts to increase significantly first. Pressure dropping gradient in the rest part of the nozzle divergent part remain relatively unchanged. As inlet vortex keeps becoming stronger, the pressure dropping gradient between locations 7&8 reaches a maximum and then starts to decrease. Meanwhile, the pressure dropping gradients in the upstream between locations 4&7 start to increase and reaches similar level as between locations 7&8 at VS=1. When the vortex strength increases from 0 to 0.34, the nozzle mass flow rate is reduced by 1.8 g/s. However, as the vortex strength increases from 0.62 to 1, the nozzle mass flow rate is only reduced by 0.3 g/s. The throat region is seen as the bottleneck of further extending vortex control range. As vortex strength increases, the pressure drop between locations 3&4 near the throat decreases due to the reduced vapor generation caused by elevated pressure and reduced liquid superheat. Therefore, nozzle throat pressure is relatively unchanged at large vortex strength and further increase of vortex strength does not reduce nozzle mass flow rate effectively.

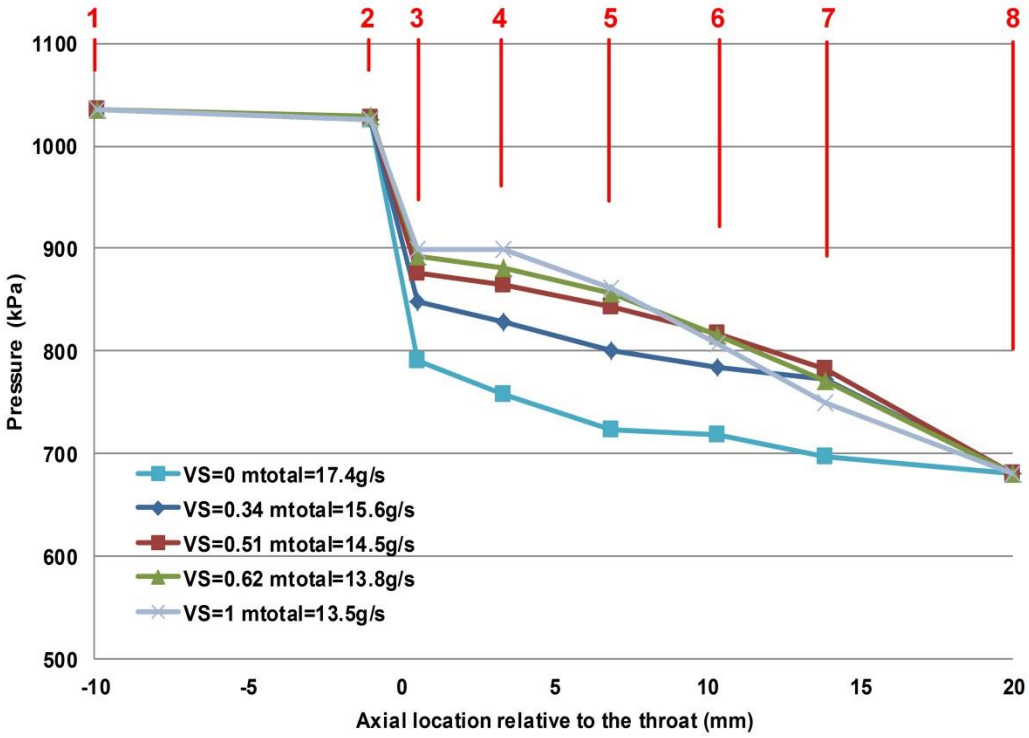

Figure 5: Influence of inlet vortex strength on the pressure at different axial locations of the nozzle with P_{in}=1035 kPa, T_{in}=40.0 °C, and P_{out}=680 kPa

Figure 6 displays the influence of inlet vapor quality on the pressure at different axial locations of the nozzle with P_{in}=925 kPa and P_{out}=680 kPa. For the subcooled inlet cases, the inlet temperature is 36.0 °C and the inlet subcooling is approximately 0.5 °C. Figure 7 shows the influence of inlet vapor quality on the nozzle total mass flow rate under abovementioned test conditions. For all the cases with non-zero inlet vapor quality, the differences of the pressure profile and the nozzle mass flow rate between the cases without and with maximum inlet vortex (same inlet vapor quality) are small, while for subcooled inlet conditions the differences are much more significant. It is believed that the vortex control effect is achieved by controlling the thermodynamic non-equilibrium of the fluid. For the cases with inlet vapor quality, due to the availability of large vapor-liquid interface area throughout the expansion in both convergent and divergent parts of the nozzle, the fluid is believed to be close to thermodynamic equilibrium. Thus the application of inlet vortex does not effectively control the thermodynamic non-equilibrium of the fluid due to the small potential and the vortex control effect is not significant. Difference between nozzle mass flow rates without and with maximum inlet vortex keeps decreasing as inlet vapor quality increases. With inlet vapor quality of 0.022, the mass flow rate difference is only 0.1 g/s. For the subcooled inlet cases, the fluid remains single-phase liquid in the convergent part even though the pressure is below saturation pressure (Zhu and Elbel, 2018a) and still has large thermodynamic non-equilibrium in the divergent part due to the lack of nucleation sites at the flow center. By applying the vortex, for subcooled inlet conditions, more vapor can be generated from the superheated liquid during the expansion in the nozzle divergent part compared with the case with no vortex, thus the fluid in the nozzle divergent part is closer to thermodynamic equilibrium than the case without vortex.

Based on the pressure profile and mass flow rate data, the vapor quality of the initially subcooled flow in the divergent part of the nozzle can be estimated with the following 1D model.

According to the previous visualization results by Zhu and Elbel (2016, 2018a), it is assumed that the fluid remains single-phase liquid in the convergent part of the nozzle and the vapor quality at location 3 is 0. Vapor and liquid velocities are assumed to be equal at each location. Pressure and axial velocity are assumed to be uniform at each cross-section. For a segment of the divergent part between locations i and j, flow mass and axial momentum balance equations are as follows:

$$\rho_i V_i A_i = \rho_j V_j A_j = \dot{m}_{total} \tag{2}$$

$$\sum F_x + \dot{m}_{total}(V_i - V_j) = 0 \quad (3)$$

where $V_{i/j}$ is the axial velocity, $\rho_{i/j}$ is assumed to be the density of thermodynamic equilibrium two-phase fluid at pressure $P_{i/j}$ and vapor quality $x_{i/j}$, $A_{i/j}$ is the flow area.

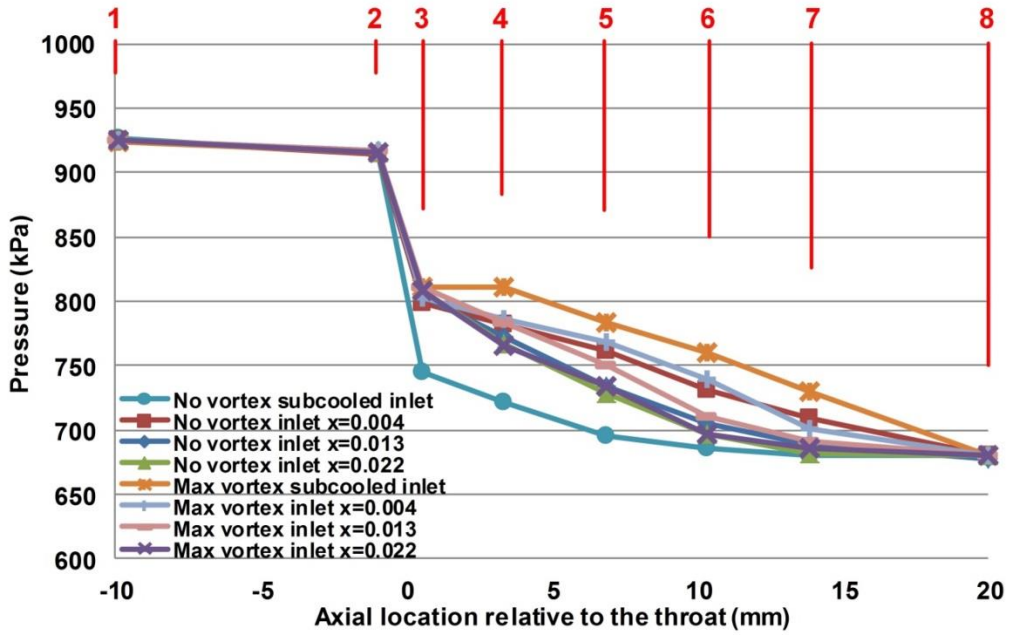

Figure 6: Influence of inlet vapor quality on the pressure at different axial locations of the nozzle with P_{in}=925 kPa and P_{out}=680 kPa

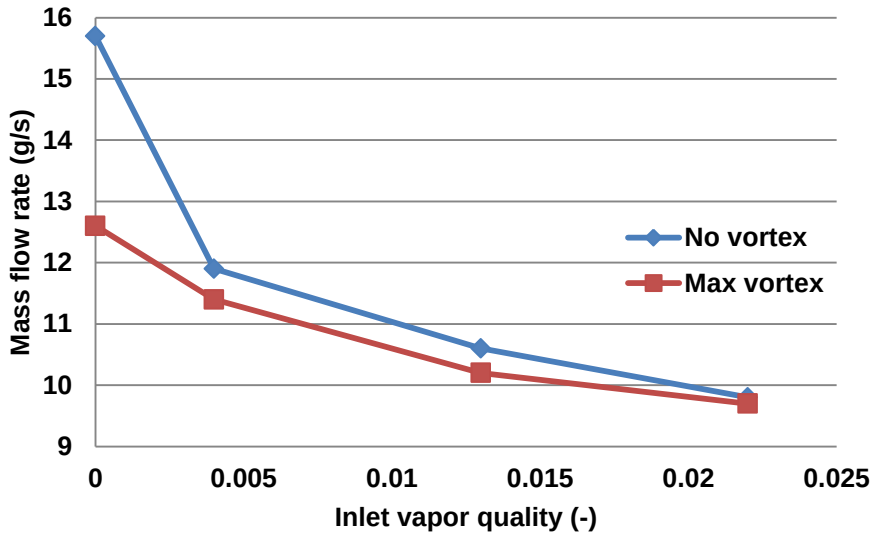

Figure 7: Influence of inlet vapor quality on the nozzle total mass flow rate with P_{in}=925 kPa and P_{out}=680 kPa

The forces considered are pressure forces and frictional force between the wall and the fluid. The frictional force is estimated with Swamee-Jain equation:

$$f = \frac{0.25}{\left[\log\left(\frac{\frac{\epsilon}{D}}{3.7} + \frac{5.74}{Re^{0.9}}\right)\right]^2} \quad (4)$$

$$\tau_w = \frac{f\rho V^2}{8} \quad (5)$$

where average values of ρ, V, D at locations i and j and liquid viscosity have been used for estimation of Reynolds number Re and wall shear stress τ_w, ϵ is the surface roughness. The nozzle inner surface roughness was measured with Dektak 3ST surface profilometer. The arithmetical mean roughness (Ra) was measured to be 1.6 μm.

Since vapor quality at location 3 has been assumed as zero, vapor quality at location 4 can therefore be computed with the above assumptions and model provided the pressure profile and mass flow rate data. Similarly the vapor quality at locations in the downstream can be computed.

Figure 8 shows the vapor quality in the divergent part at different axial locations relative to the nozzle throat estimated with the above 1D model using the measured pressure and mass flow rate data for the cases without and with maximum inlet vortex at P_{in}=925 kPa, T_{in}=36.0 °C (approximately 0.5 °C subcooling), and P_{out}=680 kPa. The thermodynamic equilibrium vapor quality assuming isentropic/isenthalpic expansion at each location is also displayed. It can be seen that the estimated vapor quality for the case with maximum inlet vortex is lower than that of the case with no vortex at locations 3&4 near the throat. As mentioned before, this is due to the elevated pressure and reduced liquid superheat such that initial vapor generation is suppressed. Between locations 5 and 8, the estimated vapor quality for the case with maximum vortex is higher than that of with no vortex. At the nozzle outlet, the estimated vapor quality for the case with maximum vortex is 0.064 which is close to the thermodynamic equilibrium vapor quality (0.082 and 0.084 for isentropic and isenthalpic expansion, respectively), while the estimated vapor quality for the case with no vortex is only 0.026. The applied vortex helps to generate more vapor in the divergent part and makes the outflow much closer to thermodynamic equilibrium.

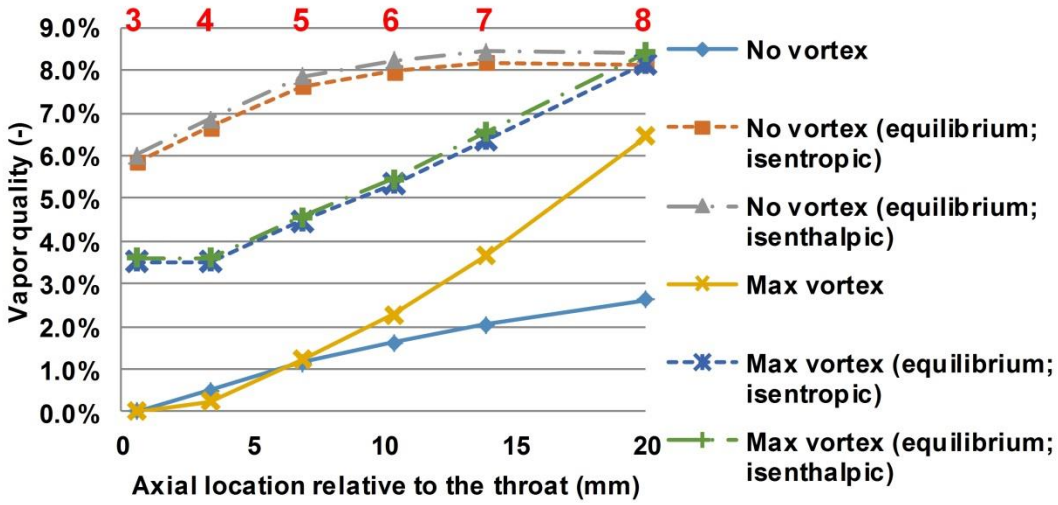

Figure 8: Estimated vapor quality and thermodynamic equilibrium vapor quality assuming isentropic/isenthalpic expansion at different axial locations for the cases without and with maximum inlet vortex at P_{in}=925 kPa, T_{in}=36.0 °C, and P_{out}=680 kPa

The estimated fluid densities at the nozzle outlet for the cases without and with maximum vortex are 625 kg/m^3 and 367 kg/m^3, respectively. Although the total mass flow rate through the nozzle with maximum vortex (12.6 g/s) is much lower than that without vortex (15.7 g/s), the fluid average axial velocity at the outlet with maximum vortex (22.3 m/s) is much higher than that without vortex (16.3 m/s) due to the much lower fluid density at the outlet. For inlet conditions of P_{in}=925 kPa and T_{in}=36.0 °C and outlet pressure of 680 kPa, the isentropic nozzle outflow velocity $V_{isentropic,out}$ is 30.2 m/s. The isentropic efficiency of a nozzle is defined as follows:

$$\eta_{\text{isentropic}} = \frac{V_{out}^2}{V_{isentropic,out}^2} \tag{6}$$

Therefore, by introduction of vortex, the isentropic efficiency of the nozzle has been improved from 29% to 55%.

4. CONCLUSIONS

In this study, measurement of the pressure profile of the vortex flashing flows in convergent-divergent nozzles under different conditions was conducted. According to the experimental results, for initially subcooled conditions the pressure drop in the divergent part of the nozzle has been increased due to the vortex. This is mainly due to the more vapor generation in the divergent part caused by the applied vortex. Since the fluid is single-phase liquid in the convergent part of the nozzle, with elevated pressure at the throat and constant inlet conditions, the nozzle mass flow rate is therefore reduced. The vortex control effect is achieved by controlling vapor generation and thus the thermodynamic non-equilibrium of the fluid. As pressure has been elevated near the throat due to the larger pressure drop in the downstream after the application of inlet vortex, liquid superheat becomes smaller and vapor generation is suppressed in the divergent part near the throat. The throat region is seen as the bottleneck of further extending vortex control range. For the cases with inlet vapor quality, due to the availability of large vapor-liquid interface area throughout the expansion in both convergent and divergent parts of the nozzle, the fluid is believed to be close to thermodynamic equilibrium. The application of inlet vortex does not effectively control the thermodynamic non-equilibrium of the fluid due to the small potential and the vortex control effect is not significant. Vapor quality at different axial locations relative to the nozzle throat has been estimated with the proposed 1D model for initially subcooled conditions based on the measured pressure profile and mass flow rates. It has been shown that the applied vortex helps to generate more vapor in the divergent part and makes the outflow much closer to thermodynamic equilibrium than without vortex. By the introduction of inlet vortex, the isentropic efficiency of the nozzle has been improved from 29% to 55%.

NOMENCLATURE

A	area	(m^2)	**Greek Symbols**		
D	diameter	(m)	ρ	density	($kg\ m^{-3}$)
F	force	(N)	τ	shear stress	(Pa)
f	friction factor	(-)			
$\dot{m}$	mass flow rate	($kg\ s^{-1}$)	**Subscript**		
P	pressure	(kPa)	axial	axial inlet	
Re	Reynolds number	(-)	f	friction	
T	temperature	(°C)	in	inlet	
V	velocity	($m\ s^{-1}$)	out	outlet	
VS	vortex strength	(-)	tangential	tangential inlet	
			w	wall	

REFERENCES

1. Zhu, J. and Elbel, S., 2016, A new control mechanism for two-phase ejector in vapor compression cycles for automotive applications using adjustable motive nozzle inlet swirl, *SAE Int. J. Passeng. Cars - Mech. Syst.*, vol. 9, no. 1: p. 44-51.
2. Zhu, J. and Elbel, S., 2017, Influence of nozzle divergent part length and throat diameter on vortex control of initially subcooled flashing flow, *SAE Int. J. Passeng. Cars - Mech. Syst.*, vol. 10, no. 1: p. 121-127.
3. Zhu, J. and Elbel, S., 2018, Experimental investigation of a novel expansion device control mechanism: Vortex control of initially subcooled flashing R134a flow expanded through convergent-divergent nozzles, *Int. J. Refrig.*, vol. 85: p. 167-183.
4. Zhu, J. and Elbel, S., 2018, CFD simulation of vortex flashing flows in convergent-divergent nozzles, *the 17th International Refrigeration and Air Conditioning Conference at Purdue*, paper 2147.

ACKNOWLEDGEMENT

The authors would like to thank the member companies of the Air Conditioning and Refrigeration Center at the University of Illinois at Urbana-Champaign for their support.